HHS Public Access

Author manuscript

Chem Eng J. Author manuscript; available in PMC 2022 December 27.

Published in final edited form as:

Chem Eng J. 2012 November 15; 211-212: 233–239. doi:10.1016/j.cej.2012.09.017.

Lead and zinc removal from aqueous solutions by aminotriphosphonate-modified converted natural phosphates

S. Saoiabi[a], **S. El Asri**[a], **A. Laghzizil**[a], **A. Saoiabi**[a], **J.L. Ackerman**[b], **T. Coradin**[c]

[a]Laboratoire de Chimie Physique Générale, Faculté des Sciences, Université Mohamed V-Agdal, BP.1014 Rabat, Morocco.

[b]Biomaterials Laboratory, Martinos Center for Biomedical Imaging, Department of Radiology, Massachusetts General Hospital and Harvard Medical School, Charlestown, MA 02129, USA

[c]UPMC Univ P6; CNRS, Chimie de la Matière Condensée de Paris, Collège de France, 75005 Paris, France

Abstract

Apatite particles prepared from natural phosphate rock and grafted with nitrilotris(methylene)triphosphonate (NTP) were evaluated for Pb^{2+} and Zn^{2+} sorption from aqueous solutions. Sorption capacities as high as 640 $mg.g^{-1}$ and 300 $mg.g^{-1}$ could be obtained for the highest organic content (10 wt%). Analysis of the sorption isotherms using Langmuir, Freundlich and Dubinin-Kaganer-Radushkevich models revealed that Pb^{2+} ions have a larger affinity for apatite (sorption energy ≈ 8 $kJ.mol^{-1}$) than for NTP so that organo-modified surfaces led to a heterogenous adsorption process. In contrast, Zn^{2+} interacts weakly (sorption energy ≈ 1 $kJ.mol^{-1}$) and similarly with the mineral surface and the organic moieties following a homogenous sorption process. Such an association of organic metal ligands with reactive apatite surfaces within porous materials appears as a promising strategy to obtain efficient adsorbents at low cost and limited environmental impact.

Keywords

Natural Phosphate; Apatite; Porous material; Surface functionalization; heavy metals

1. Introduction

Heavy metals are of special environmental concern because they are non-degradable and therefore persistent [1]. They are toxic in both their elemental form and within mineral structures, even at low concentrations [2]. Among available heavy metal remediation methods, chemical precipitation has long been favoured [3]. Although other techniques such as ion exchange [4], membrane systems [5], and electrodeposition [6] have been widely developed over the last few decades, adsorption processes is considered as the most attractive alternative to chemical precipitation [7], not only because it is well-adapted to the treatment of wastewaters containing high concentrations of metals [8] but also because a wide variety of adsorbents such as activated carbon [9], clays [10], silica [11] as well as natural and synthetic apatites [12–16] are available.

Among these adsorbents, natural phosphate rock combines the advantages of very low cost, low environmental impact and great abundance, with well-known affinity of hydroxyl and phosphate groups for metallic cations [17]. However, they exhibit a limited porosity that limits their use as such for metal sorption applications [18–19]. Moreover, apatite surfaces exhibit a positively charged surface in acidic conditions that decreases their affinity for metal cations in polluted waters [20]. To address these points, we recently developed a novel procedure for the preparation of mesoporous organo-apatite materials derived from natural phosphate (modified natural phosphate, MNP), by incorporation of nitrilotris(methylene)triphosphonic acid (NTP) exhibiting amine and phosphonate surface moieties (Fig. 1) [21–22]. The introduction of amine groups was based on previous reports showing that apatite materials grafted with aminosilanes exhibit enhance retention properties towards Cu^{2+} and Co^{2+}, due to complexation between $-NH_2$ and metal ions [23–24]. Indeed, Pb^{2+} ions represent a specific case when considering apatite-based adsorbents because they are known to interact with apatite surface via dissolution and precipitation of pyromorphite $Pb_{10}(PO_4)_6(X)_2$ (X = OH, Cl) phases [12, 25]. Therefore, a balance may exist in the Pb^{2+} sorption efficiency between the benefits of introducing metal-binding ligands and the decreased accessibility of the apatite surface. For instance, it was previously shown that polyacrylamide-modified apatites exhibited improved affinity towards the UO_2^{2+} and Th^{4+} ions, whereas the retention of Pb^{2+} was hindered by the presence of the polymer [26]. Accordingly, polyurethane foams incorporating apatite particles were also described exhibiting increased Pb^{2+} retention capacity but slower Pb^{2+} sorption kinetics with apatite content [27].

On this basis, we have here studied Pb^{2+} sorption on MNP materials modified with increasing amounts of NTP. Langmuir, Freundlich and Dubinin-Kaganer-Radushkevich models have been evaluated to model adsorption isotherms. The pH variations during the sorption process were also monitored to get a better understanding of the ongoing phenomena. In parallel, the sorption of another metal ion, Zn^{2+}, with lower affinity for apatite surface was also studied and compared to that of Pb^{2+}.

2. Experimental

2.1. Synthesis of NTP-modified natural phosphate nanoparticles (NTP-MNP)

NTP-MNP powders were synthesized from natural phosphate from Bengurir, Morocco and NTP, as described elsewhere [22, 28]. As summarized in Fig. 2, 500 mL of deionized water adjusted to pH 2 with HNO_3 (65%) solution was used to dissolve 20.6 g natural phosphate (−400/+100 μm fraction after sieving) by stirring for 3 hours. After filtration, reagent grade nitrilotris(methylene)triphosphonic acid (50 wt.% water solution, Sigma-Aldrich, St. Louis, MO) was added to the clear solution under vigorous stirring. The resulting transparent mixture was precipitated with concentrated ammonia (25%) at pH 10, resulting in a white suspension. This suspension was aged for 24 h at room temperature, filtered, washed with deionized water, and dried overnight at 100 °C.

XRD patterns of as-prepared materials after drying at 100°C are shown in Fig. 3a. A poorly crystalline structure is obtained for all products, with typical diffraction peaks at $2\theta \approx 32°$, 33° and 34° corresponding to the (211), (112) and (300) planes of the apatite structure

(JCPDS No. 09–0432). A significant broadening of diffraction peaks suggests reduction in apatite crystallinity in the presence of increasing amount of organic molecules. FTIR spectra of the various products display the vibration modes of [PO_4] groups at 1100, 1050, 960, 605 and 565 cm^{-1} characteristic of the apatite structure (Fig. 3b). The broadening of PO_4 bands with NTP content is related to the structural disorder and the presence of R-PO_3 groups [29]. The FT-IR spectra of the composites exhibit weak peaks in the 1400–1450 cm^{-1} wavenumber range, corresponding to organic C-C vibrations whereas MNP shows a large band in the same region indicating that MNP is a carbonated apatite. This indicates that phosphonate groups of NTP substitute carbonate ions in the apatite structure upon grafting. The grafting of NTP is also supported by the presence of a wide band in the 2500–3000 cm^{-1}, resulting from the overlap of the C–H, N-C and C-P stretching band of NTP.

N_2-sorption experiments show the presence of an hysteresis loop for all samples, indicating that the materials are mesoporous (Fig. 4a). However, the nitrogen sorption isotherm of MNP show a clear threshold at high relative pressure, that becomes less significant for 2.5 %-NTP and 5%-NTP and disappears for 10%-NTP, suggesting the opening of the mesoporous network with increasing organic modification. Transmission Electron Microscopy Imaging show that all materials consist of nanoparticles whose size, *ca.* 50 nm, does not clearly depend on the NTP content (Fig. 4b,c). Further characterizations are available elsewhere [22]. Main chemical and structural features of the organo-apatites are gathered in Table 1.

2.2. Adsorption procedure

Aqueous solutions containing Pb^{2+} and Zn^{2+} ions at various concentrations were prepared from lead and zinc nitrate in distilled water. Adsorption isotherms were determined in a 500 mL thermostatted reactor by mixing 100 mL of metal-containing solution with 0.2 g of adsorbent at 25°C. The mixture was stirred at 400 rpm for 3 h to allow the adsorption to reach equilibrium, using a mechanical stirrer (EUROSTAR digital IKA) to provide reproducible and homogeneous mixing. The initial metal concentration was varied from 10 to 2000 mg L^{-1}. The initial pH was adjusted to pH 5. The variation of the pH of the contaminated aqueous solutions during metal adsorption was measured for all adsorbents using a pH meter (METTLER TOLEDO equipped with a glass electrode), with experimental variations in a 2% range. Pb^{2+} sorption kinetics were measured by the same procedure at predefined times, but using 200 mL of Pb^{2+} solution with 0.4 g of adsorbent. Aliquots of the supernatant solution were taken with a 2 mL propylene syringe equipped with a 0.45 μm filter. The amount of adsorbed lead per gram of adsorbent q_t (in mg g^{-1}) at time t was calculated as follows:

$$q_t = \frac{C_0 - C_t}{m} V \quad (1)$$

where C_0 and C_t are the metal ion concentration (in mg L^{-1}) in the liquid phase initially and at any time t respectively, m is the mass of adsorbent (in g) in the solution, and V is the solution volume (in L). All measurements were performed in triplicate and experimental errors were found below 5%. Lead, and zinc elements were

chemically analyzed by inductively coupled plasma atomic emission spectroscopy (ICP-AES) (ICPS-7500, Shimadzu, Japan).

2.3 Kinetics of metal sorption

In order to determine the rate constants, the two most widely used kinetic models of adsorption (Lagergren pseudo-first and pseudo-second order models) were applied to the experimental data [29]. The Lagergren pseudo-first order equation can be expressed as:

$$log(q_{e,1} - q_t) = \log q_{e,1} - \frac{k_1}{2.303}t \quad (2)$$

where $q_{e,1}$ is the amount of adsorbed metal per gram of adsorbent (in mg g^{-1}) at equilibrium, t is reaction time (in s) and k_1 is the pseudo-first order rate constant. This model is applicable if $\log(q_{e,1} - q_t)$ versus t approximates a straight line, in which case $q_{e,1}$ and k_1 can be calculated. The pseudo-second order model can be expressed as:

$$\frac{t}{q_t} = \frac{1}{k_2 q_{e,2}^2} + \frac{1}{q_{e,2}}t \quad (3)$$

If this model is applicable, the plot of t/q_t against time t in Eq. (3) will yield a linear relationship from which the constants $q_{e,2}$, the amount of adsorbed metal per gram of adsorbent (in mg g^{-1}) at equilibrium and k_2 the pseudo-second order rate constant can be determined from the intercept and slope of the plot $t/q_t = f(t)$. The fitting procedure was performed using the Kaleidagraph software that provides coefficient of determination R^2 and χ^2 parameters, from which $\chi_{red}^2 = \chi^2$/(number of experimental points-2).

2.4. Modeling of the adsorption isotherms

Langmuir, Freundlich and Dubinin-Kagener-Radushkevich models are commonly used to study sorption processes [30]. The Langmuir model is based on the assumption that a maximum uptake exists, corresponding to a saturated monolayer of sorbed molecules on the adsorbent surface. In this model, all adsorption sites have the same adsorption energy, no interaction exists between adsorbed molecules, and the limiting reaction step is the surface reaction, as in a heterogeneous catalytic reaction. The Langmuir equation can be written as:

$$q_e = q_{e,max}\frac{K_L C_e}{1 + K_L C_e} \quad (4)$$

where q_e is the amount of sorbed metal at equilibrium (mg.g^{-1}), $q_{e,max}$ is the maximum sorption capacity (mg.g^{-1}), K_L is the equilibrium constant of the adsorption reaction and (L. mg^{-1}), C_e is the equilibrium concentration of metals remaining in solution (mg.L^{-1}).

The Freundlich model assumes that adsorption occurs on a heterogeneous surface through a multilayer adsorption mechanism and that the adsorbed amount increases with the concentration according to Xu et al. [25]:

$$q_e = q_{e,max}\frac{K_F C_e^{\beta}}{1 + K_F C_e^{\beta}} \quad (5)$$

where K_F is the equilibrium constant of the adsorption reaction and β is the empirical parameter related to the intensity of adsorption, which varies with the heterogeneity of the material. When β values are from 0.1 to 1, the adsorption conditions are favourable.

The Dubinin-Kaganer-Radushkevich model can be used to describe the characteristic porosity of the adsorbent as well as the apparent energy of adsorption. The DKR model may be represented as:

$$q'_e = q'_{e,max} exp\left(\frac{RT}{\sqrt{2E}} ln\left(1 + \frac{1}{C'_e}\right)\right)^2 \quad (6)$$

where q'_e is the amount of sorbed metal at equilibrium (mol.g^{-1}), $q'_{e,max}$ is the maximum sorption capacity (mol.g^{-1}), C'_e is the equilibrium concentration of metals remaining in solution (mol.L^{-1}) and E the adsorption energy (in J.mol^{-1} for R = 8.31 J.mol^{-1}.K^{-1} and T temperature in K).

3. Results and discussion

3.1. Pb^{2+} sorption

The time-dependent behavior of Pb^{2+} adsorption was examined by varying the incubation time of the Pb^{2+}/apatite mixture at a temperature of 25 °C (Fig. 5). For ungrafted MNP materials, the adsorption curve is smooth, with maximum sorption being reached after *ca.* 2 hours. Pb^{2+} depletion from solution by the modified apatites occurs much more rapidly and saturation is reached after 60 min and 50 min for 2.5% NTP-MNP and 5% NTP-MNP, respectively). An increase of NTP up to 10 % does not modify further the sorption kinetics (data not shown).

Table 2 gathers the parameters derived from the application of the Lagergren pseudo first-order ($q_{e,1}$ and k_1) and pseudo second-order ($q_{e,2}$ and k_2) kinetic models. As already mentioned, it was difficult to obtain a reasonable fitting of the experimental data for the MNP material using these models. For the grafted systems, the first-order model appeared suitable to reproduce the experimental data (Fig. 5) with reasonable values of the coefficient of determination R^2, in contrast to the second-order equation. The adsorption rate constant k_1 increases by a factor 5 in the presence of 2.5 wt% NTP and less significantly for a higher organic content. The maximum capacities were found similar for all samples, although reduced χ^2_{red} values were too high to fully conclude on this point.

Based on the kinetics data, the contact time to establish equilibrium was selected at 3 h. Fig. 6 shows isotherms describing the equilibrium adsorption capacity q_e as a function of Pb^{2+} concentration for various NTP-MNP adsorbents. From the experimental maximum capacities, q_{max}, it can be noted that the NTP-grafted MNP particles have greater ability to

remove Pb^{2+} ions from aqueous solution compared to ungrafted MNP, with a remarkable increase in sorption capacity from 2.5 wt% to 5 wt% NTP content (Table 3).

Langmuir and Freundlich models were evaluated to simulate the sorption isotherms, using the linearized form of the equations. On the one hand, the Langmuir model appears well-adapted for the pure MNP material as well as for low NTP content (2.5 wt%), with R^2 values close to unity (Table 3) and good agreement between the calculated curve and the experimental data (Fig. 6). In contrast, higher organic grafting density led to poor simulation and low R^2 values. On the contrary, the Freundlich model was poorly adapted to NMP and 2.5 % NTP-MNP but reproduces in a reasonable manner the sorption data obtained for 5 wt% and 10 wt% NTP content (Fig. 6). These observations reflect that the homogeneity of initial apatite surface that is only slightly perturbed by low organic content, being therefore suitable simulated by the Langmuir isotherm. Higher organic density leads to an inhomogeneous surface whose sorption behavior is therefore more accurately modeled by the Freundlich equation.

The DKR equation was also evaluated (Table 3). No accurate simulation of the pure apatite phase could be obtained, especially indicating a low $q_{e,max}$, which might reflect that the well-known formation of pyromorphite phases by surface dissolution-reprecipitation process [12, 25] may invalidate DKR model. In contrast, much better agreement was obtained with organically-modified apatites. The calculated $q_{e,max}$ values were similar to experimental data and results from Langmuir/Freundlich-based simulation. It can also be noticed that calculated interaction energies, that are in the range of previous reports on metal sorption on apatite [31–32], decrease from 8 $kJ.mol^{-1}$ to 4 $kJ.mol^{-1}$ with increasing NTP content. Although the calculated value for MNP is to be taken carefully, this decrease suggests that the interaction between the ligand and Pb^{2+} is not stronger than the one between the apatite surface and metal ions. Therefore, the observed increase in the amount of adsorbed metal with NTP density must be related to the introduction of additional binding sites.

The evolution of the pH of the solution during the Pb^{2+}-sorption process was also monitored (Fig. 7). The pure apatite material shows a fast increase of solution pH from 5 to 7.9, reflecting protonation of the phosphate groups, as well as surface dissolution leading to the release of hydroxide ions. In the presence of NTP, the pH increase is more limited (6.9–7.1), as the combined effect of smaller available apatite surface and of the presence of amine functions with high pK_a values [33]. When Pb^{2+} ions are present, a lower final pH value (6.4) is obtained for pure apatite. This can be attributed to the interactions of Pb^{2+} with phosphate groups that not only are less available for protonation by water molecules but may even release some protons due to $PO_4^-\ldots H^+ \leftrightarrow Pb^{2+}$ exchange. Noticeably, the final pH also decreases with increasing NTP content. Above-mentioned explanations, *i.e.* smaller available apatite surface due to surface grafting and Pb^{2+} interactions with phosphate groups of the apatite surface are still applying here. In addition, protons may be released when Pb^{2+} interact with the phosphate and amine group of the NTP molecules [34]. Finally, it is important to note that the pKa of the $Pb^{2+}/Pb(OH)^+$ system is 7.71 [35], so that 95% of lead species are in the divalent state. Hence the observed pH increase is not expected to impact significantly on the efficiency of the adsorption process.

3.2. Comparison with Zn^{2+} sorption

In order to understand better the relative contribution of the apatite surface and organic ligand to the sorption capacity of the composite materials, the sorption of Zn^{2+}, a divalent cation with low affinity for apatite, was also studied. Sorption isotherms are shown on Fig. 8. Compared to Pb^{2+}, experimental maximum capacities q_{max} were significantly lower, by nearly a factor of 2 for pure apatite and 10 %NTP-MNP. In addition, the increase of Zn^{2+} sorption with NTP content appears more continuous than for Pb^{2+}, especially the difference between maximum sorption capacity of 2.5% and 5 %NTP-MNP samples is less marked for Zn^{2+} compared to Pb^{2+}. However, it has to be considered that comparison must be established on the basis of moles of metals rather than weight. In this case, the q'_{max} values are 1.6 $mmol.g^{-1}$ and 3.1 $mmol.g^{-1}$ for Pb^{2+} and 2.3 $mmol.g^{-1}$ and 4.6 $mmol.g^{-1}$ for Zn^{2+} on pure apatite and 10w%NTP-MNP, respectively.

Another important difference was observed when Langmuir and Freundlich isotherms were evaluated for simulation of experimental data. For Zn^{2+}, all data were accurately reproduced by the Langmuir equation (Fig. 8) whereas Freundlich model was less adapted, as indicated by R^2 values. Use of the DKR model revealed suitable to simulate Zn^{2+} sorption on pure apatite, supporting our previous hypothesis about the interference of the specific interaction between Pb^{2+} and apatite on the application of this model. In the presence of NTP, the sorption energy is not significantly modified compared to the pure apatite. All together, this suggests that the surface of the material appears homogeneous towards Zn^{2+} sorption, independently of the presence of the NTP molecules. It is worth noting that the sorption energy for Zn^{2+} is significantly smaller than for Pb^{2+}. This correlates well with the fact that Pb^{2+} is well-known for its strong interaction with apatite, a process that does not occur readily with Zn^{2+}. When pH variation is examined for the pure apatite, one can notice a lower final pH for Zn^{2+} than for Pb^{2+}, which is in agreement with the fact that more Zn^{2+} are adsorbed than Pb^{2+} (Fig. 7). For 5 %NTP-MNP, a decrease in pH is observed in the presence of Zn^{2+} compared to pure apatite, as already observed for Pb^{2+}. However, the final pH is higher than for Pb^{2+}, which can be due to the weaker interaction energy between Zn^{2+} and the surface, limiting the extent of the metal ion with protonated phosphate and amine groups. It is worth noting that the $Zn^{2+}/Zn(OH)^{+}$ system has a pKa of 8.96 [35], so that more than 99 % of zinc species are in the divalent state at the equilibrium pH. This may enhance zinc adsorption compared to lead. Another important point is related to the possible precipitation of hopetite [$Zn_3(PO_4)_2.4H_2O$] in these acidic conditions, that can contribute to Zn^{2+} removal from the solution [36]. Whereas such a precipitation cannot be ruled out, the suitable fitting of sorption data by the Langmuir model suggests that the apatite surface is homogeneous for Zn^{2+} and therefore this process is not significant.

Finally, it is interesting to note that here-obtained maximum capacity (> 600 $mg.g^{-1}$ for Pb^{2+}) overpass by far all previously reported data (*ca.* 100 $mg.g^{-1}$) for Pb^{2+} sorption by natural and synthetic apatites [15, 27, 37–39] as well as by activated carbons [40] or zeolites [41]. This is due to our ability to incorporate organic moieties without decreasing the specific surface area of the material, in contrast to other previous studies dedicated to organo-apatites [26–27].

4. Conclusion

The incorporation of NTP within the apatite powder increases its affinity for both Pb^{2+} and Zn^{2+}. Because Pb^{2+} exhibits a strong and specific affinity (ionic exchange and surface precipitation) for the apatite surface, the presence of NTP molecules introduces some heterogeneity in the sorption process. Therefore the increase in sorption capacity with NTP content is due to the introduction of additional binding sites for Pb^{2+} ions but these sites, phosphate and/or amine groups of NTP, have a lower affinity than the apatite surface for these ions. In contrast, Zn^{2+} has a similar and low affinity for both apatite and NTP so that the accessible surface remains homogeneous upon ligand incorporation. Here again, NTP incorporation provides additional binding sites for metal sorption. Hence, the overall sorption capacity results from a delicate balance between the relative affinity of apatite and NTP for the metal ions.

The high sorption capacities obtained here indicate that the proposed strategy is promising. The fact that the apatite was obtained from a natural phosphate rock is also a key advantage due to its low cost and limited environmental impact. Despite its low price, the substitution of NTP by some natural binding molecules, such as carboxylates [42], may be preferred for future development and scaling-up and is currently under study. In addition, it is important to note that, for both Pb^{2+} and Zn^{2+}, the reversible sorption process occurs simultaneously to the precipitation of a metal phosphate phase, pyromorphite or hopetite. At this time, it is difficult to evaluate the relative contribution of the two processes. However, this should be investigated in more details if recyclable materials are to be designed.

References

[1]. Linak WP, Wendt JOL, Toxic metal emissions from incineration: mechanisms and control, Prog. Energy Combust. Sci 19 (1993) 145–185.

[2]. Pain DJ, Amiard-Trinquet C, Lead poisoning of raptors in France and elsewhere. Ecotoxicol. Environ. Safety, 25 (1993) 183–192. [PubMed: 7682502]

[3]. Mulligan CN, Young RN, Gibbs BF, An evaluation of technologies for the heavy metal remediation of dredged sediments, J. Hazard Mater 85 (2001) 145–163. [PubMed: 11463508]

[4]. Zhu Y, Millan E, Sengupta AK, Towards separation of toxic metal (IT) cations by chelating polymers: some noteworthy observations, Reactive Polym. 13 (1990) 241–253.

[5]. Blöcher C, Dorda J, Mavrov V, Chmiel H, Lazaridis NK, Matis KA, Hybrid flotation–membrane filtration process for the removal of heavy metal ions from wastewater, Water Res. 37 (2003) 4018–4026. [PubMed: 12909122]

[6]. Hatfield TL, Pierce DT, Electrochemical remediation of metal-bearing wastewaters. Part I: copper removal from simulated mine drainage waters, J. Appl. Electrochem 26 (1996) 567–574.

[7]. Montinaro S, Concas A, Pisu M, Cao G, Immobilization of heavy metals III: contaminated soils through ball milling with and without additives, Chem. Eng. J 142 (2008) 271–284.

[8]. Basta T, McGowen SL, Evaluation of chemical immobilization treatments for reducing heavy metal transport in a smelter–contaminated soil, Environ. Poll 127 (2004) 73–82.

[9]. Leyva Ramos R, Bernal Jacome LA, Mendoza Barron J, Fuentes Rubio L, Guerrero Coronado RM, Adsorption of zinc (II) from an aqueous solution onto activated carbon, J. Hazard. Mater 90 (2002) 27–38. [PubMed: 11777590]

[10]. Singh SP, Ma LQ, Hendry MJ, Characterization of aqueous lead removal by phosphatic clay: Equilibrium and kinetics studies, J. Hazard Mater B136 (2006) 654–662.

[11]. Aguado J, Arsuaga JM, Arencibia A, Lindo M, Gascón V, Aqueous heavy metals removal by adsorption on amine–functionalized mesoporous silica, J. Hazard. Mater 163 (2009) 213–221. [PubMed: 18675509]

[12]. Ma QY, Traina SJ, Logan TJ, Ryan JA, In situ lead immobilization by apatite, Environ. Sci. Technol 27 (1993) 1803–1810.

[13]. Valsami-Jones E, Ragnarsdottir KV, Putnis A, Bosbach D, Kemp AJ, Cressey G, The dissolution of apatite in the presence of aqueous metal cations at pH 2–7, Chem. Geol 151 (1998) 215–233.

[14]. Cao X, Ma LQ, Rhue DR, Appel CS, Mechanisms of lead, copper, and zinc retention by phosphate rock, Environ. Pollut 131 (2004) 435–444. [PubMed: 15261407]

[15]. Mouflih M, Aklil A, Sebtib S, Removal of lead from aqueous solutions by activated phosphate, J. Hazard. Mater B119 (2005) 183–188.

[16]. El Hammari L, Laghzizil A, Saoiabi A, Barboux P, Meyer M, Brandès S, Guilard R, Some factors affecting the removal of lead from aqueous solution by porous calcium hydroxyapatite: relationships between structural and adsorption properties, Ads. Sci. Technol 24 (2006) 507–516.

[17]. Elouear Z, Bouzid J, Boujelben N, Feki M, Jamoussi F, Montiel A, Heavy metal removal from aqueous solutions by activated phosphate rock, J. Hazard. Mater 156 (2007) 412–420. [PubMed: 18242833]

[18]. El Asri S, Laghzizil A, Coradin T, Saoiabi A, Alaoui A, M'hamedi R, Conversion of natural phosphate rock into mesoporous hydroxyapatite for heavy metals removal from aqueous solution, Colloid Surf. A: Physicochem. Eng. Aspects 362 (2010) 33–38.

[19]. Kaludjerovic-Radoicic T, Raicevic S, Aqueous Pb sorption by synthetic and natural apatite: kinetics, equilibrium and thermodynamic studies, Chem. Eng. J 160 (2010) 503–510.

[20]. Bengtsson A, Shchukarev A, Persson P, Sjöberg S, A solubility and surface complexation study of a non-stoichiometric hydroxyapatite, Geochim. Cosmochim. Acta 73 (2009) 257–267.

[21]. Saoiabi S, El Asri S, Laghzizil A, Coradin T, Lahlil K, Nanoporous surface of organofunctionalized hydroxyapatite fabricated from natural phosphate rock, Mater. Lett 64 (2010) 2679–2681.

[22]. Saoiabi S, EL Asri S, Laghzizil A, Masse S, Ackerman JL, Lahlil K, Synthesis and characterization of nanoapatites organofunctionalized with aminotriphosphonate agents, J. Solid State Chem 185 (2012) 95–100. [PubMed: 22287800]

[23]. Chiron N, Guilet R, Deydier EC, Adsorption of Cu (II) and Pb (II) onto a grafted silica: isotherms and kinetic models, Water Res. 37 (2003) 3079–3086. [PubMed: 14509694]

[24]. da Silva OG, da Silva Filho EC, da Fonseca MG, Arakaki LNH, Airoldi C, Hydroxyapatite organofunctionalized with silylating agents to heavy cation removal, J. Colloid Interf. Sci 302 (2006) 485–491.

[25]. Xu H, Yang L, Wang P, Liu Y, Peng M, Kinetic research on the sorption of aqueous lead by synthetic carbonate hydroxyapatite, J. Environ. Manag 86 (2008) 319–328.

[26]. Ulusoy U, Akkaya R, Adsorptive features of polyacrylamide–apatite composite for Pb^{2+}, UO_2^{2+} and Th^{4+}, J. Hazard. Mater 163 (2009) 98–108. [PubMed: 18656311]

[27]. Jang SH, Min BG, Jeong YG, Lyoo WS, Lee SC, Removal of lead ions in aqueous solution by hydroxyapatite/polyurethane composite foams, J. Hazard. Mater 152 (2008) 1285–1292. [PubMed: 17850963]

[28]. El Asri S, Laghzizil A, Saoiabi A, Alaoui A, El Abbassi K, M'hamdi R, Hakam A, Coradin T, A novel process for the fabrication of nanoporous apatites from Moroccan phosphate rock, Colloid Surf. A: Physicochem. Eng. Aspects 350 (2009) 73–78.

[29]. Ho YS, Review of second-order models for adsorption systems, J. Hazard. Mater 136 (2006) 681–689. [PubMed: 16460877]

[30]. Dron J, Dodi A, Comparison of adsorption equilibrium models for the study of Cl^-, NO_3^- and SO_4^{2-} removal from aqueous solutions by an anion exchange resin. J. Hazard. Mater 190 (2011) 300–307. [PubMed: 21497015]

[31]. Smiciklas I, Dimovic S, Plecas I, Mitric M, Removal of Co^{2+} from aqueous solutions by hydroxyapatite, Water Res. 40 (2006) 2267–2274. [PubMed: 16766010]

[32]. Wang Y-J, Chen J-H, Cui YX, Wang S-Q, Zhou D-M, Effects of low-molecular-weight organic acids on Cu (II) adsorption onto hydroxyapatite nanoparticles, J. Hazard. Mater 162 (2009) 1135–1140. [PubMed: 18614282]

[33]. Popov A, Rönkkömäki H, Popov K, Lauri HLajunen J, Vendilo A, ^{31}P NMR protonation equilibrium study of iminobis(methylenephosphonic acid) and its derivatives at high pH, Inorg. Chim. Acta, 353 (2003) 1–7.

[34]. Cabeza A, Aranda MAG, Bruque S, New lead triphosphonates: synthesis, properties and crystal structures, J. Mater. Chem 9 (1999) 571–578.

[35]. Pagnanelli F, Esposito A, Toro L, Veglio F, Metal speciation and pH effect on Pb, Cu, Zn and Cd biosorption onto *Sphaerotilus natans*: Langmuir-type model, Water Res. 37 (2003) 627–633. [PubMed: 12688697]

[36]. Lee YJ, Elzinga EJ, Reeder RJ, Sorption mechanisms of zinc on hydroxyapatite: systematic uptake studies and EXAFS spectroscopy analysis, Environ. Sci. Technol 39 (2005) 4042–4048. [PubMed: 15984781]

[37]. Liao D, Zheng W, Li X, Yang Q, Yue X, Guo L, Zeng G, Removal of lead (II) from aqueous solutions using carbonate hydroxyapatite extracted from eggshell waste, J. Hazard. Mater 177 (2010) 126–130. [PubMed: 20042291]

[38]. Jiang S-D, Yao Q-Z, Zhou G-T, Fu S-Q, Fabrication of hydroxyapatite hierarchical hollow microspheres and potential application in water treatment, J. Phys. Chem. C 116 (2012) 4484–4492.

[39]. Sasaki T, Sakai Y, Iizuka A, Nakae T, Kato S, Kojima T, Yamasaki A, Evaluation of the capacity of hydroxyapatite prepared from concrete sludge to remove lead from water, Ind. Eng. Chem. Res 50 (2011) 9564–9568

[40]. Sekar M, Sakhti V, Rengaraj S, Kinetics and equilibrium adsorption study of lead (II) onto activated carbon prepared from coconut shell, J. Colloid Interf. Sci 279 (2004) 307–313.

[41]. Shawabkeh R, Al-Harahsheh A, Hami M, Khlaifat A, Conversion of oil shale ash into zeolite for cadmium and lead removal from wastewater, Fuel 83 (2004) 981–985.

[42]. Achelhi K, Masse S, Laurent G, Saoiabi A, Laghzizil A, Coradin T, Role of carboxylate chelating agents on the chemical, structural and textural properties of hydroxyapatite, Dalton Trans. 39 (2010) 10644–10651. [PubMed: 20886132]

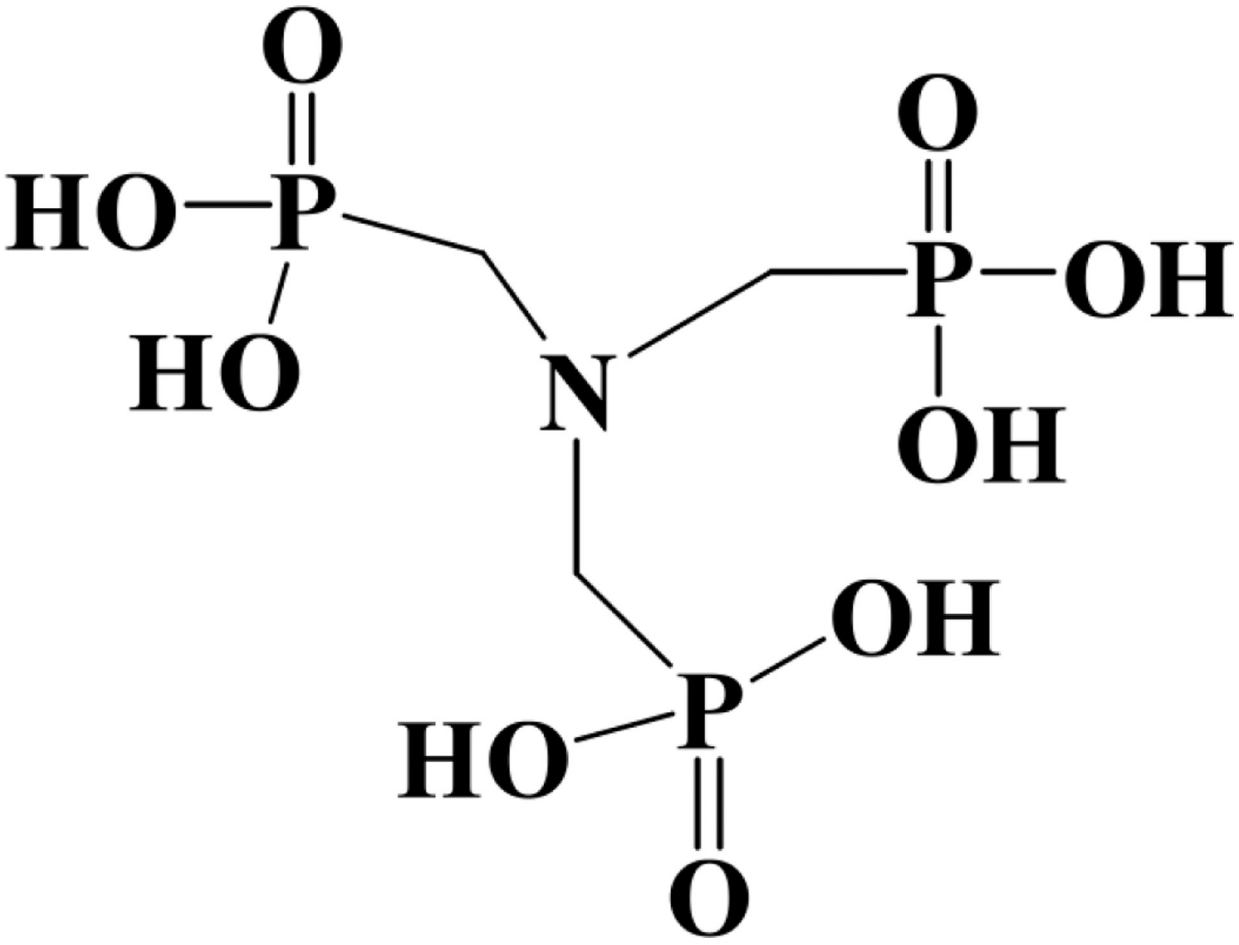

Figure 1.
Structure of nitrilotris(methylene)triphosphonic acid.

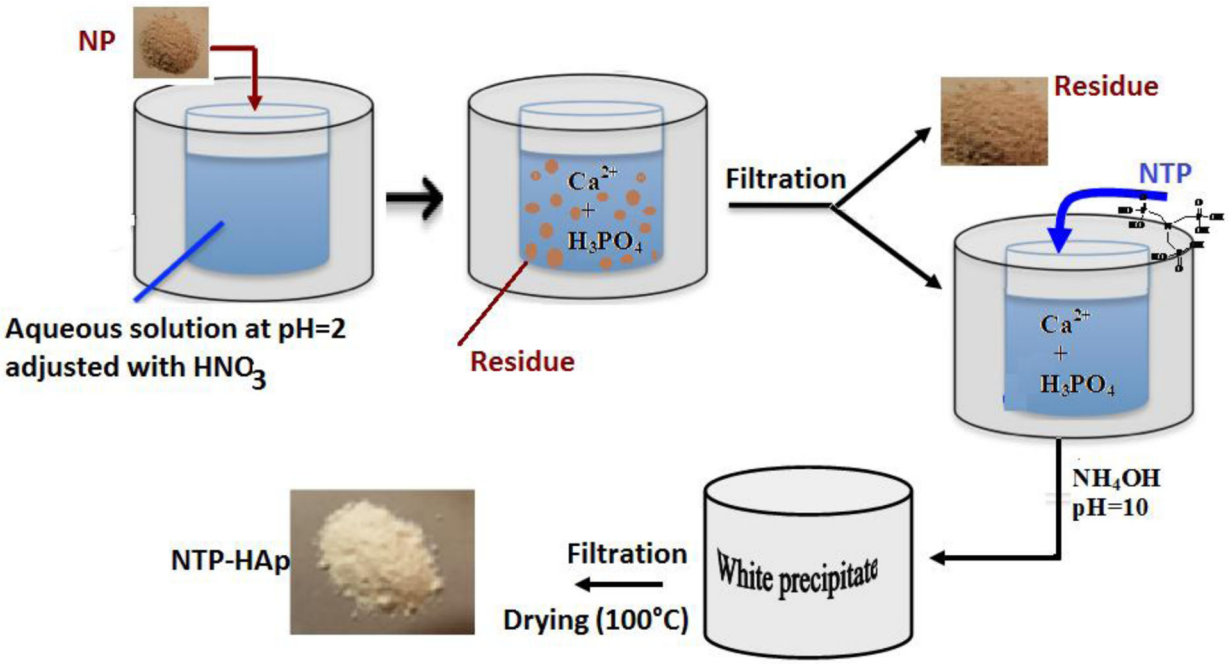

Figure 2.
Overview of the synthetic route to NTP-MNP apatites

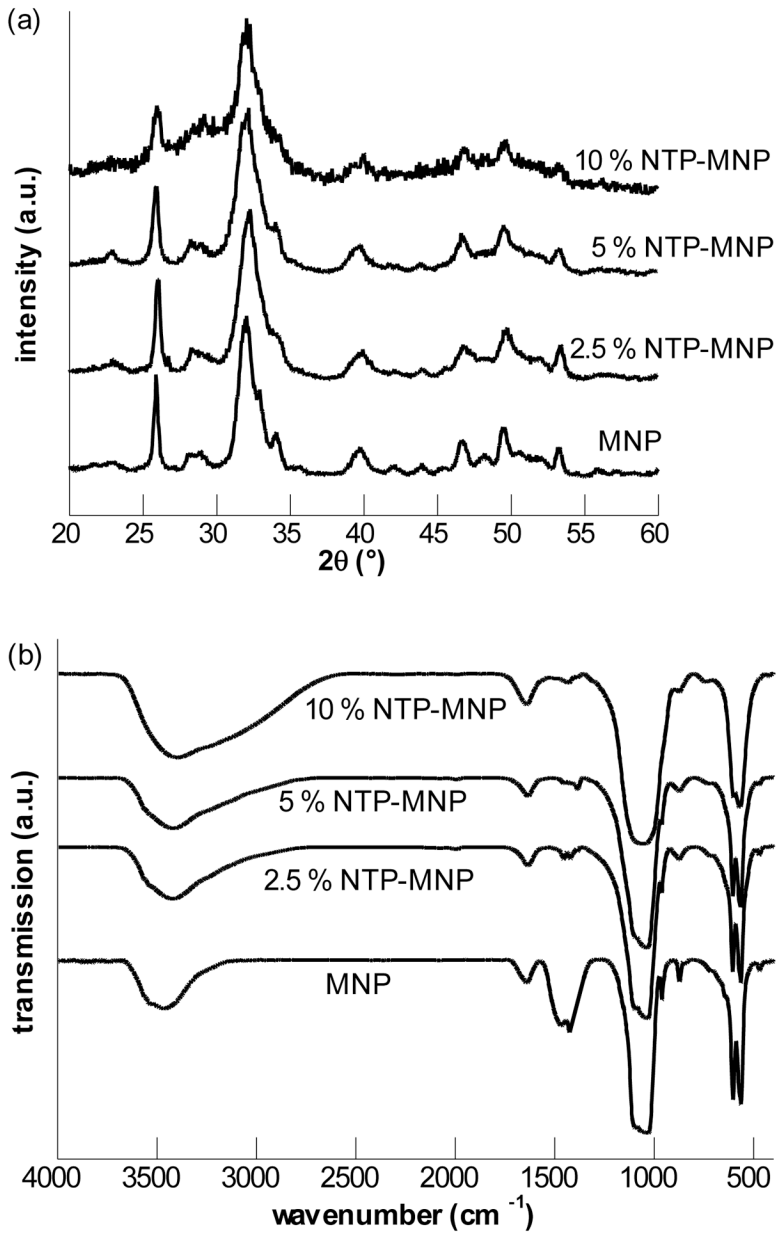

Figure 3.
(a) XRD diffractograms and (b) FTIR spectra of NTP-MNP apatites with varying NTP content

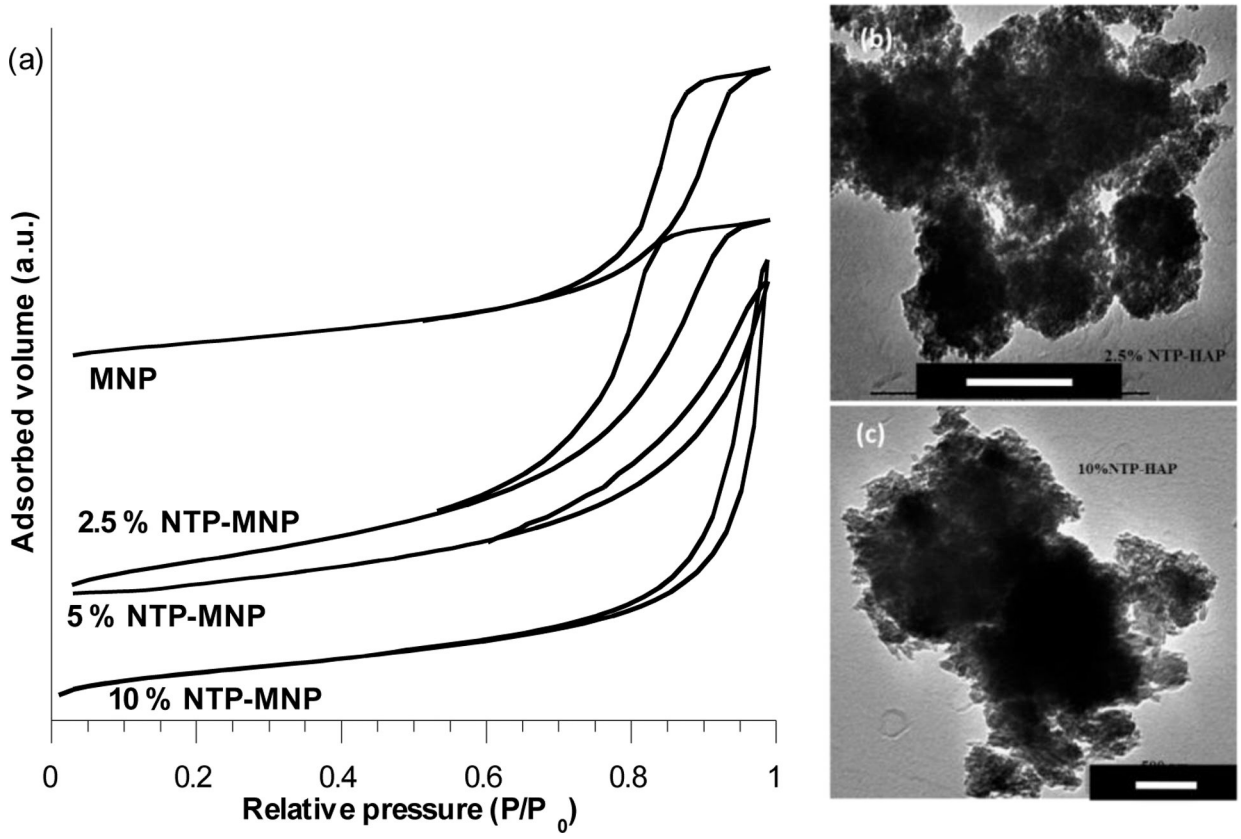

Figure 4.

(a) N_2-sorption isotherms at 77 K onto NTP-MNP apatite with varying NTP content; TEM images of (b) 2.5 % NTP-MNP and (c) 5%NTP-MNP (scale bar = 200 nm).

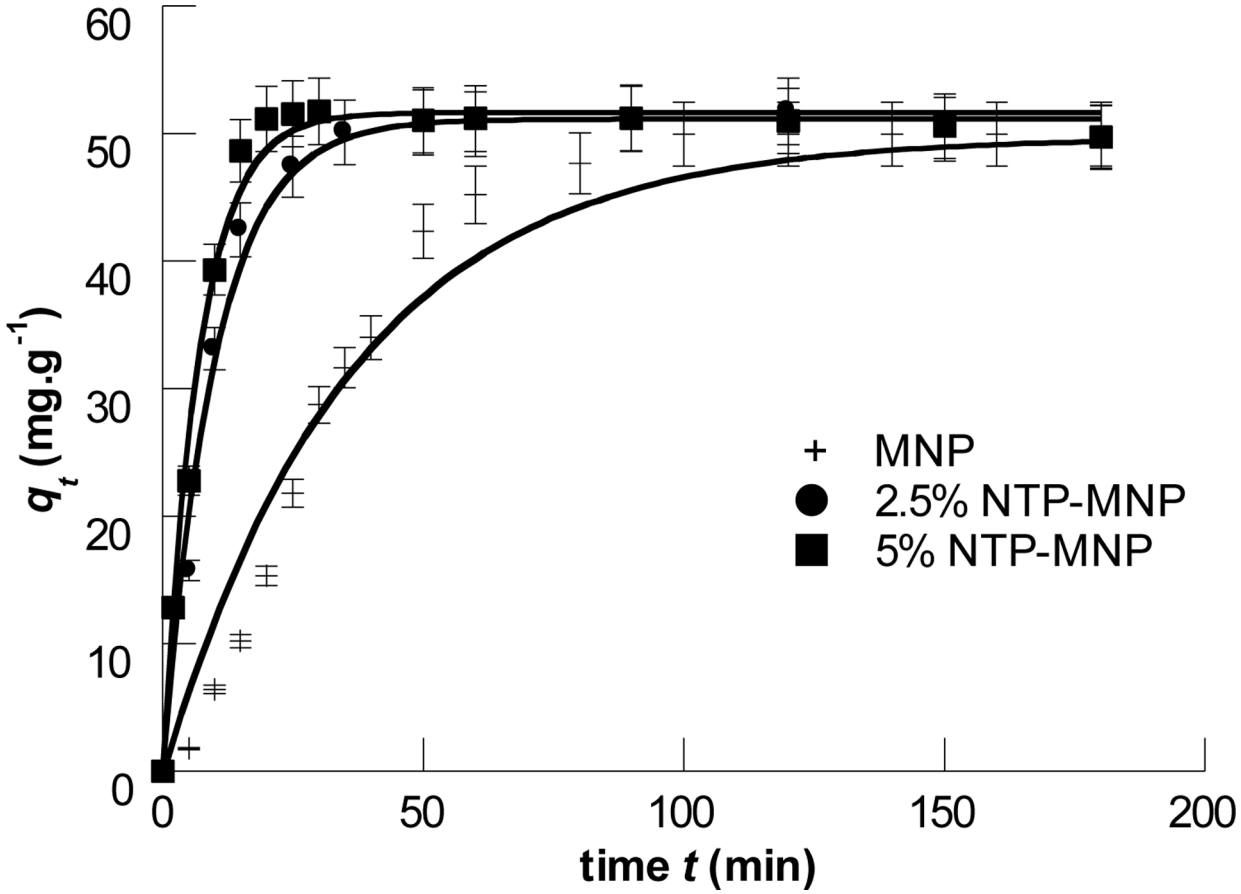

Figure 5.
Effect of incubation time on Pb^{2+} adsorption q_t onto NTP-MNP apatite with varying NTP content.

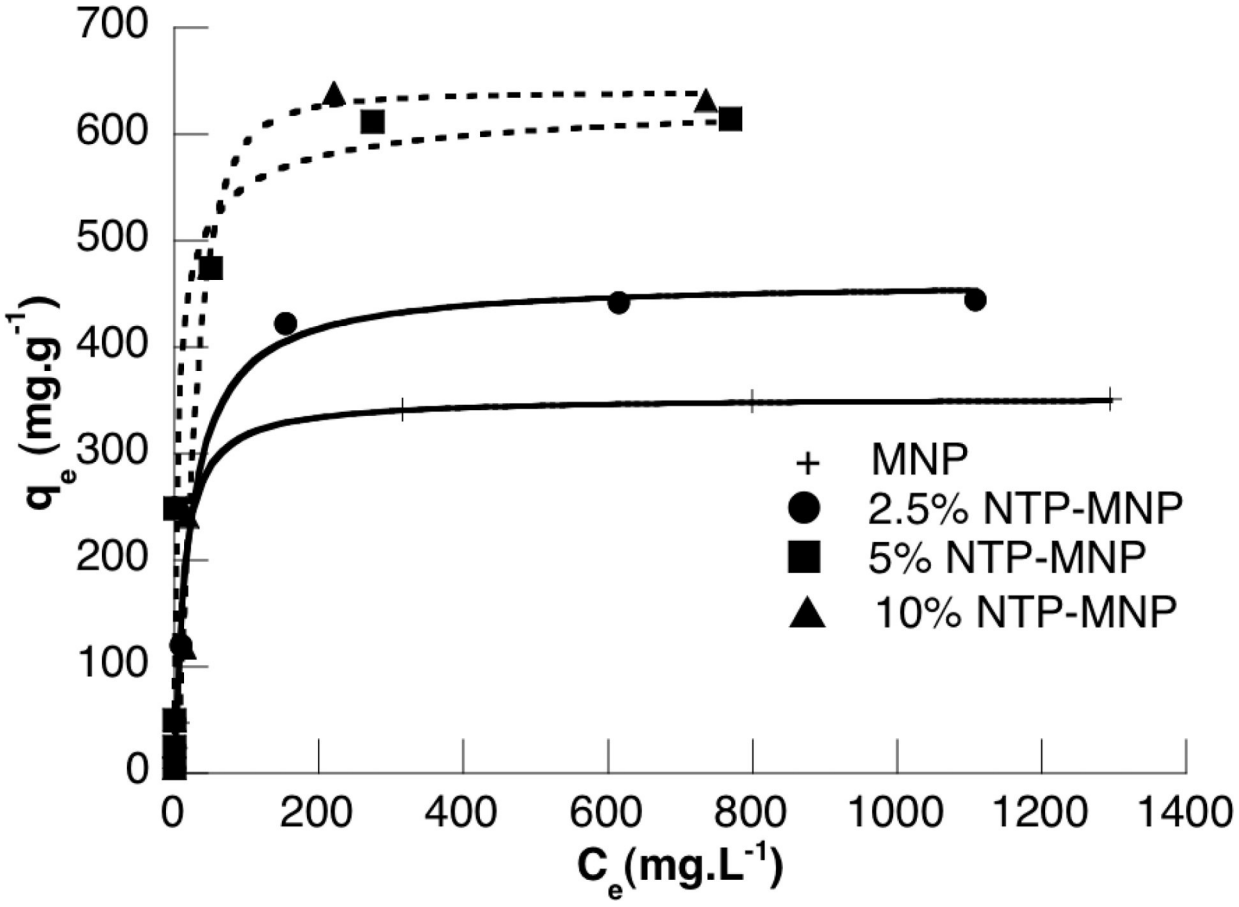

Figure 6.

Variation of sorbed Pb^{2+} content q_e with metal concentration C_e at equilibrium onto NTP-MNP with various NTP contents. Plain and dashed lines represent curve fitting using Langmuir and Freundlich model, respectively.

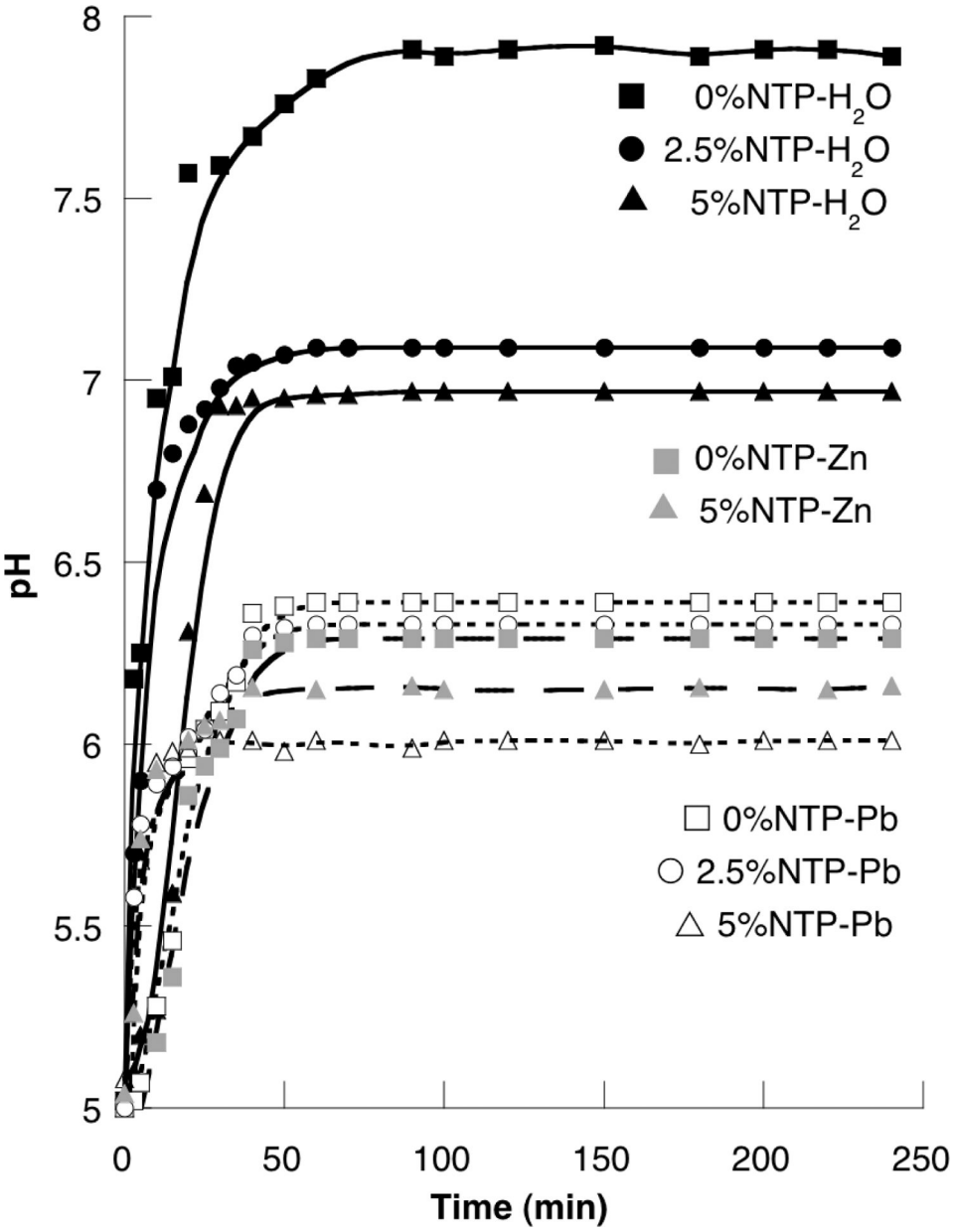

Figure 7.

Equilibrium pH change in the presence of ungrafted MNP and NTP-grafted MNP with acidified water (pH 5, dark symbols), added Pb^{2+} (open symbols) and added Zn^{2+} (grey symbols). Lines are provided as guides only.

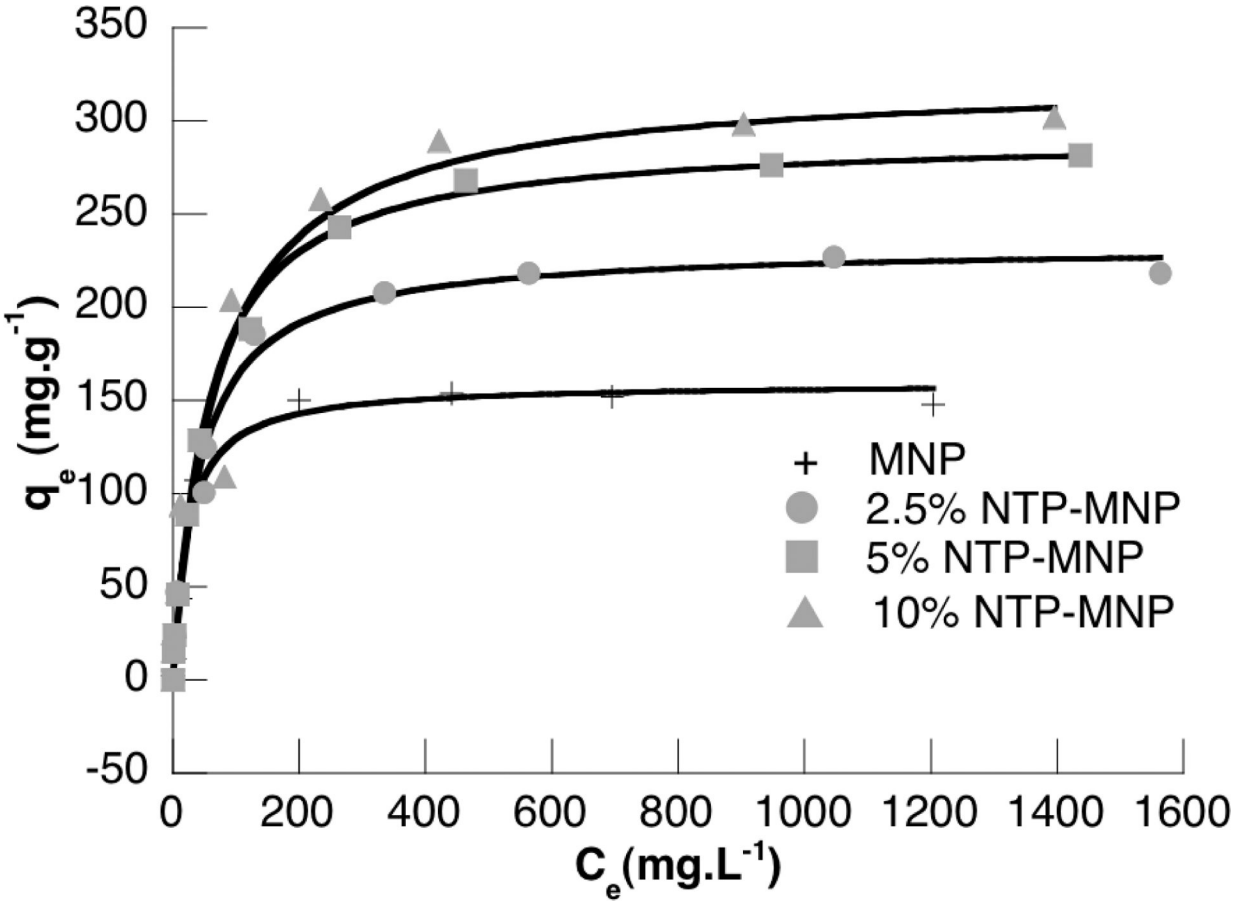

Figure 8.

Variation of adsorbed Zn^{2+} content q_e with metal concentration C_e at equilibrium onto NTP-MNP with various NTP contents. Plain lines represent curve fitting using Langmuir model.

Table 1.

Chemical composition and porous characteristics of pure and graft-modified apatites: calcium/phosphorus molar ratio (Ca/P), total organic carbon (%C) and nitrogen (%N), specific surface area S_{BET} and average pore diameter (D_p).

NTP (%)	Ca/P	% C	% N	S_{BET} ($m^2.g^{-1}$)[a]	D_p (nm)
0	1.95	0.30	-	150	10
2.5	1.61	0.52	0.20	200	10
5	1.55	0.72	0.32	150	25
10	1.53	1.05	0.62	145	40

[a] $\pm$ 5 $m^2.g^{-1}$

Table 2.

Kinetic rate constants and adsorption capacities computed using Lagergren pseudo first and second order models for Pb^{2+} adsorption on pure and NTP-modified phosphates.

Lagergren model		**NTP content (%)**		
		0	**2.5**	**5**
First order	$q_{e,1}$ ($mg.g^{-1}$)	50 ± 2	51 ± 1	51 ± 1
	k_1 (min^{-1})	0.025 ± 0.005	0.100 ± 0.005	0.140 ± 0.005
	$_R2$	0.980	0.995	0.992
	χ_{red}^2	> 2	1.2	1.5
Second order	$q_{e,2}$ ($mg.g^{-1)}$	50 ± 5	55 ± 2	55 ± 2
	k_2 ($mg.min^{-1}$)	0.0003 ± 0.0001	0.002 ± 0.001	0.004 ± 0.001
	R_2	0.973	0.978	0.978
	χ_{red}^2	> 2	> 2	> 2

Table 3:

Langmuir, Freundlich and Dubinin-Kaganer-Radushkevich constants for Pb^{2+} NTP-MNP and pure MNP apatite as reference.

Model		NTP content (%)			
		0	**2.5**	**5**	**10**
Experimental	q_{max} (mg.g^{-1})	330	445	615	640
Langmuir	$q_{e,max}$ (mg.g^{-1})	350 ± 20	460 ± 20	580 ± 30	700 ± 50
	K_L	0.10 ± 0.05	0.05 ± 0.02	0.6 ± 0.2	0.03 ± 0.01
	R^2	0.998	0.998	0.988	0.984
Freundlich	$q_{e,max}$ (mg.g^{-1})	600 ± 100	1000 ± 400	640 ± 50	640 ± 20
	β	0.3 ± 0.2	0.3 ± 0.2	0.6 ± 0.1	0.8 ± 0.1
	K_F	0.1 ± 0.4	0.1 ± 0.4	0.4 ± 0.1	0.02 ± 0.01
	R^2	0.851	0.873	0.994	0.996
Experimental	q'_{max} (mmol.g^{-1})	1.6	2.1	3.0	3.1
	$q'_{e,max}$ (mmol.g^{-1})	1.6 ± 0.2	2.1 ± 0.1	2.9 ± 0.1	3.2 ± 0.1
DKR	E (kJ.mol^{-1})	7 ± 1	5 ± 1	4 ± 0.1	4 ± 0.1
	R^2	0.825	0.967	0.983	0.992

Table 4:

Langmuir, Freundlich and Dubinin-Kaganer -Radushkevich constants for Zn^{2+} NTP-MNP and pure MNP apatite as reference.

		NTP content (%)			
		0	**2.5**	**5**	**10**
Experimental	q_{max} (mg.g^{-1})	150	225	280	300
	$q_{e,max}$ (mg.g^{-1})	160 ± 5	230 ± 10	290 ± 5	320 ± 20
Langmuir	K_L	0.04 ± 0.01	0.03 ± 0.01	0.02 ± 0.01	0.01 ± 0.01
	R^2	0.998	0.998	0.998	0.993
Freundlich	$q_{e,max}$ (mg.g^{-1})	150 ± 10	240 ± 20	300 ± 10	370 ± 70
	β	1.4 ± 0.1	0.7 ± 0.1	0.8 ± 0.1	0.7 ± 0.2
	K_F	0.02 ± 0.01	0.06 ± 0.02	0.03 ± 0.01	0.05 ± 0.03
	R^2	0.979	0.992	0.990	0.976
Experimental	q'_{max} (mmol.g^{-1})	2.3	3.5	4.3	4.6
	$q'_{e,max}$ (mmol.g^{-1})	2.3 ± 0.1	3.5 ± 0.1	4.2 ± 0.2	4.6 ± 0.2
DKR	E (kJ.mol^{-1})	1.2 ± 0.5	0.8 ± 0.1	0.8 ± 0.1	0.8 ± 0.1
	R^2	0.992	0.967	0.983	0.992